

Dipolar spin ice states with fast monopole hopping rate in CdEr_2X_4 ($\text{X} = \text{Se}, \text{S}$)

Shang Gao,^{1,2} Oksana Zaharko,^{1,*} Vladimir Tsurkan,^{3,4} Lilian Prodan,⁴ Edward Riordan,⁵ Jorge Lago,⁶ Björn Fåk,⁷ Andrew Wildes,⁷ Marek M. Koza,⁷ Clemens Ritter,⁷ Peter Fouquet,⁷ Lukas Keller,¹ Emmanuel Canévet,¹ Marisa Medarde,⁸ Jakob Blomgren,⁹ Christer Johansson,⁹ Sean R. Giblin,⁵ Stanislav Vrtnik,¹⁰ Jože Luzar,¹⁰ Alois Loidl,³ Christian Rüegg,^{1,2} and Tom Fennell^{1,†}

¹Laboratory for Neutron Scattering and Imaging,

Paul Scherrer Institut, CH-5232 Villigen PSI, Switzerland

²Department of Quantum Matter Physics, University of Geneva, CH-1211 Geneva, Switzerland

³Experimental Physics V, University of Augsburg, D-86135 Augsburg, Germany

⁴Institute of Applied Physics, Academy of Sciences of Moldova, MD-2028 Chisinau, Republic of Moldova

⁵School of Physics and Astronomy, Cardiff University, CF24 3AA Cardiff, United Kingdom

⁶Department of Inorganic Chemistry, Universidad del País Vasco (UPV-EHU), 48080 Bilbao, Spain

⁷Institut Laue-Langevin, F-38042 Grenoble, France

⁸Laboratory for Scientific Developments and Novel Materials,

Paul Scherrer Institut, CH-5232 Villigen PSI, Switzerland

⁹RISE Acreo AB, SE-411 33 Göteborg, Sweden

¹⁰Jožef Stefan Institute, SI-1000 Ljubljana, Slovenia

(Dated: October 4, 2022)

Excitations in a spin ice behave as magnetic monopoles, and their population and mobility control the dynamics of a spin ice at low temperature. CdEr_2Se_4 is reported to have the Pauling entropy characteristic of a spin ice, but, surprisingly, its dynamics are three-orders of magnitude faster than the canonical rare earth titanate spin ice $\text{Dy}_2\text{Ti}_2\text{O}_7$. In this letter we use diffuse neutron scattering to show that both CdEr_2Se_4 and CdEr_2S_4 support a dipolar spin ice state – the host phase for a Coulomb gas of emergent magnetic monopoles. At low temperatures these Coulomb gases have similar parameters to that in $\text{Dy}_2\text{Ti}_2\text{O}_7$, *i.e.* dilute and uncorrelated, so cannot provide three-orders faster dynamics through a larger monopole population. We investigate the monopole dynamics using ac susceptometry and neutron spin echo spectroscopy, and verify the crystal electric field Hamiltonian of the Er^{3+} ions using inelastic neutron scattering. We find that a calculation of the monopole hopping rate using our Coulomb gas and crystal electric field parameters quantitatively reproduces the fast dynamics in CdEr_2X_4 ($\text{X} = \text{Se}, \text{S}$). Our work shows that CdEr_2X_4 are dilute magnetic Coulomb gases with high monopole mobility.

A magnetic Coulomb phase is characterized by an effective magnetic field whose topological defects behave as emergent magnetic monopoles [1]. In dipolar spin ices such as $\text{Dy}_2\text{Ti}_2\text{O}_7$, where long-range dipolar interactions between spins on the pyrochlore lattice establish the two-in-two-out ice rule (which gives the field its non-divergent character) [2], the monopoles are deconfined and interact according to a magnetic Coulomb law [3–5]. The transformation from the spin model to a Coulomb gas of magnetic monopoles simplifies the understanding of the properties of dipolar spin ices as the complicated couplings among the spins are replaced by the determinant parameters of the Coulomb gas: the elementary charge Q_m , chemical potential v_0 , and hopping rate u [3, 6]. Through analogs with Debye-Hückel theory of Coulomb gases, many thermodynamic observables can be conveniently calculated [7–9].

The spin relaxation rate of canonical spin ices was a particular problem in the spin representation. From high to low temperature it changes from thermally activated, to a temperature independent plateau, to a re-entrant thermally activated regime [10–13]. At high temperature, above the monopole regime, Orbach processes describe the thermally activated relaxation rate [13]. The plateau

and re-entrant thermally activated regimes do not have a ready explanation in the spin representation, and can only now be understood as the hopping of monopoles by quantum tunneling in screened and unscreened regimes of the Coulomb gas respectively [11, 12]. In the unscreened regime, the relaxation rate depends on the monopole density ρ with the hopping rate u as the coefficient: $f \propto \rho u$ when the system is near equilibrium [7, 8, 14].

Although the monopole charge Q_m and chemical potential v_0 can be calculated exactly from the spin model, the value of the monopole hopping rate u is not well-understood and is usually treated as a fitting parameter [11, 12, 15]. For $\text{Dy}_2\text{Ti}_2\text{O}_7$, u is fitted to be $\sim 10^3$ Hz at $T < 12$ K, which has been experimentally confirmed through the Wien effect [6]. Recently, Tomasello *et al* found that this hopping rate can be estimated by the splitting of the crystal-electric-field (CEF) ground state doublet under an internal transverse magnetic field of 0.1–1 T [16]. To verify the universality of this approach, it is beneficial to compare the monopole dynamics in other dipolar spin ice compounds.

The newly proposed spin ice state in the spinel CdEr_2Se_4 provides such an opportunity [17–19]. In this compound, Er^{3+} ions constitute the pyrochlore lat-

tice, and bulk measurements have revealed the remnant Pauling entropy and local Ising character for the Er^{3+} spins [17, 18]; both are strong indicators of the existence of the spin ice state although microscopic evidence is required to confirm its dipolar character. Of special importance is the low-temperature dynamics in CdEr_2Se_4 , which was revealed to be three-orders faster than that of the pyrochlore titanate $\text{Dy}_2\text{Ti}_2\text{O}_7$ [18]. The origin of this increase and its compatibility with monopole dynamics in CdEr_2Se_4 remains unclear.

In this letter, we explore the spin ice states and their monopole dynamics in CdEr_2X_4 ($X = \text{Se}, \text{S}$). Using inelastic neutron scattering to study the CEF transitions and neutron diffuse scattering to study the spin correlations, we provide the microscopic evidence for the existence of the dipolar spin ice states in CdEr_2X_4 . Through ac susceptibility measurements, we reveal fast monopole dynamics in the whole quantum tunneling regime. Comparison with a calculation of the splitting of the Er^{3+} CEF ground state doublet under perturbative transverse fields reveals the increase of the monopole hopping rate as the main contribution to the fast dynamics. Thus our work explains the fast monopole dynamics in CdEr_2X_4 and provides general support to this monopole hopping mechanism in dipolar spin ices.

Our powder samples of CdEr_2Se_4 and CdEr_2S_4 were synthesized by the solid state reaction method [20]. To reduce neutron absorption, the ^{114}Cd isotope was used. X-ray diffraction measurements confirmed the good quality of our samples, with the Er_xX_y impurities less than 1 %. Inelastic neutron scattering experiments were performed on IN4 with 1.21 and 2.41 Å incident neutron wavelengths at Institut Laue-Langevin (ILL). Polarized neutron diffuse scattering experiments were performed on CdEr_2Se_4 using D7 with a 4.8 Å setup at ILL. Non-polarized neutron diffuse scattering experiments were performed on CdEr_2S_4 using DMC with a 2.46 Å setup at SINQ of Paul Scherrer Insitut (PSI). Neutron spin echo experiments were performed on IN11 at ILL. AC susceptibilities χ in the frequency range of $1\text{--}1 \times 10^3$ Hz were measured with the Quantum Design MPMS SQUID at Laboratory for Scientific Developments and Novel Materials of PSI. AC susceptibilities in the frequency range of $2.5 \times 10^4\text{--}5.5 \times 10^6$ Hz were measured using a bespoke induction ac susceptometer.

Fig. 1 presents the inelastic neutron scattering results of the CEF transitions in CdEr_2Se_4 and CdEr_2S_4 . Altogether 6 peaks are observed at the base temperature for both compounds, which is consistent with the Stokes transitions within the $\text{Er}^{3+} {}^4I_{15/2}$ manifold under D_{3d} symmetry. Using the McPhase program [21], we fitted the measured spectra with the CEF Hamiltonian $H = \sum_{lm} B_l^m \hat{O}_l^m$, where \hat{O}_l^m are the Stevens operators and B_l^m are the corresponding coefficients. The fitting results are shown in Fig. 1 as the solid lines and Table I lists the fitted CEF parameters and ground state wave-

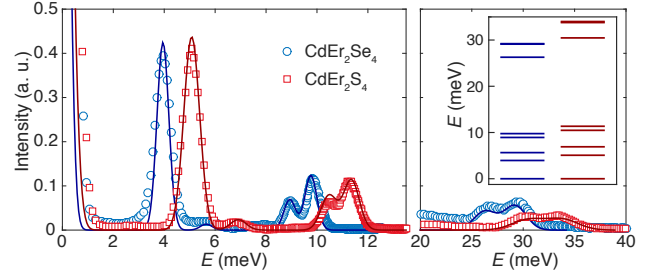


FIG. 1. (color online). Inelastic neutron scattering results of the CEF transitions in CdEr_2Se_4 (measured at $T = 2$ K) and CdEr_2S_4 (measured at $T = 1.5$ K). Error bars are smaller than the symbol size. The fits are shown as the solid lines. The inset shows the fitted energies of the CEF levels for CdEr_2Se_4 (left column) and CdEr_2S_4 (right column).

TABLE I. The fitted Wybourne CEF parameters (meV) and ground state doublets for CdEr_2Se_4 and CdEr_2S_4 .

	B_2^0	B_4^0	B_4^3	B_6^0	B_6^3	B_6^6
CdEr_2Se_4	-25.70	-107.73	-97.74	25.31	-19.06	9.51
CdEr_2S_4	-29.18	-122.72	-113.66	25.97	-21.89	14.41
J_z	$\pm 15/2$	$\pm 9/2$	$\pm 3/2$	$\mp 3/2$	$\mp 9/2$	
CdEr_2Se_4	± 0.906	0.386	± 0.159	-0.073	± 0.004	
CdEr_2S_4	± 0.904	0.391	± 0.145	-0.094	± 0.006	

functions. For both compounds, the ground states transform as the $\Gamma_5^+ \oplus \Gamma_6^+$ dipole-octupole doublet [22, 23]. Specifically, the wavefunctions for both of the ground state doublets are dominated by the $|7.5, \pm 7.5\rangle$ components and have almost the same anisotropic g -factors of $g_\perp = 0$ and $g_\parallel = 16.4$, which is consistent with the previous report for CdEr_2Se_4 [18]. Thus our inelastic neutron scattering results confirm the Ising character of the Er^{3+} spins in CdEr_2Se_4 and CdEr_2S_4 .

Although the Pauling entropy is a strong signature of the spin ice state in CdEr_2Se_4 [18], it only characterizes the spin configurations at the length scale of a single tetrahedron. To realize a magnetic Coulomb gas with interacting monopoles, it is essential to have a dipolar spin ice state with power-law spin correlations, which can be verified through measurements of the spin correlations [4]. Fig. 2 presents the quasi-static spin-spin correlations in CdEr_2Se_4 obtained from polarized neutron diffuse scattering [24]. Broad peaks are observed at 0.6 and 1.4 Å⁻¹, and the overall pattern is very similar to that of the known dipolar spin ices [25–27]. Sharp peaks with very weak intensities are also discernible near 1.1 Å⁻¹ and can be attributed to the magnetic Bragg peaks of the Er_xSe_y impurities [20].

To fit the observed spin-spin correlations in CdEr_2Se_4 , we performed single-spin-flip Monte Carlo simulations for the dipolar spin ice model with exchange couplings up to

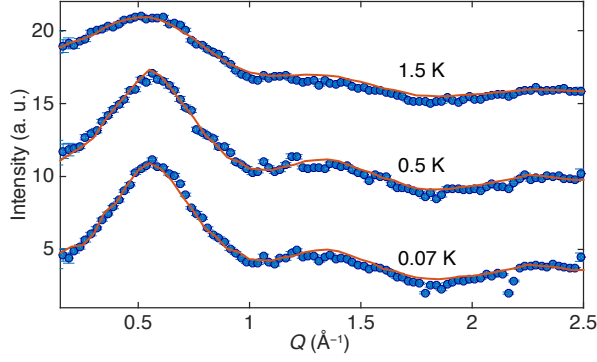


FIG. 2. (color online). CdEr_2Se_4 magnetic scattering at 0.07, 0.5, and 1.5 K obtained from the xyz polarization analysis. The 0.5 (1.5) K data is shifted by 6 (12) along the y axis. The Monte Carlo simulation results are shown as the solid red lines.

the second neighbors [28]:

$$\mathcal{H} = J_1 \sum_{\langle ij \rangle} \sigma_i \sigma_j + J_2 \sum_{\langle\langle ij \rangle\rangle} \sigma_i \sigma_j + Dr_0^3 \sum_{ij} \left[\frac{\vec{n}_i \cdot \vec{n}_j}{|r_{ij}|^3} - \frac{3(\vec{n}_i \cdot \vec{r}_{ij})(\vec{n}_j \cdot \vec{r}_{ij})}{|r_{ij}|^5} \right] \sigma_i \sigma_j. \quad (1)$$

Here, \vec{n}_i is the unit vector along the local $\langle 111 \rangle$ axes with the positive direction pointing from one diamond sublattice of the tetrahedra center to the other, $\sigma_i = \pm 1$ is the corresponding Ising variable, J_1 and J_2 are the exchange interactions for nearest neighbors (NN) $\langle ij \rangle$ and second-nearest neighbors $\langle\langle ij \rangle\rangle$, respectively, r_0 is the NN distance, and $D = \mu_0(\langle J_z \rangle g \mu_B)^2 / (4\pi r_0^3)$ is the dipolar interaction, 0.616 and 0.690 K for CdEr_2Se_4 and CdEr_2S_4 , respectively. With the ALPS package [29], we implemented the Hamiltonian (1) on a $6 \times 6 \times 6$ supercell with periodic boundary conditions. The dipolar interaction was truncated beyond the distance of 3 unit cells. The spin-spin correlations were evaluated every 100 sweeps during the 4×10^5 sweeps of measurement. Assuming the effective NN coupling $J_{\text{eff}} = J_1 + 5D/3$ to be equal to 1 K at which temperature the CdEr_2Se_4 specific heat maximum was observed [18, 30, 31], we fixed J_1 to -0.027 K and only varied J_2 in the fitting process. As is shown in Fig. 2, the model with $J_2 = 0.042$ K fits the measured spin correlations very well. We found no need to include J_3 , which appears in other dipolar spin ices [28]. Although the exact value of J_2 might be susceptible to both of the supercell size and the dipolar cutoff, our simulations do confirm the dominance of the dipolar interactions in CdEr_2Se_4 . Non-polarized neutron diffuse scattering results for CdEr_2S_4 are shown in the Supplemental Material [20], which have similar Q -dependence as that of CdEr_2Se_4 and can be fitted by the dipolar spin ice model as well. In this way, we establish the existence of the dipolar spin ice state in CdEr_2Se_4 and CdEr_2S_4 .

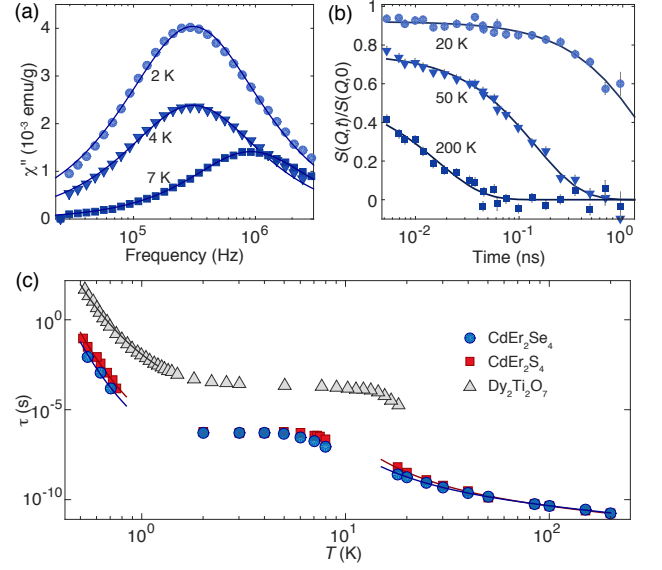


FIG. 3. (color online). (a) Imaginary parts of the ac susceptibilities of CdEr_2Se_4 measured at 2, 4, and 7 K with the Cole-Cole model fits shown as the solid lines. (b) Normalized spin echo intermediate scattering function $S(Q, t)/S(Q, 0)$ of CdEr_2Se_4 measured at 20, 50, and 200 K with the fits shown as the solid lines. (c) Extracted relaxation time in CdEr_2Se_4 and CdEr_2S_4 . Error bars are smaller than the symbol sizes. The Arrhenius (Orbach) fits in the low (high) temperature regime are shown as the solid lines. Relaxation rates together with the low-temperature Arrhenius fits for $\text{Dy}_2\text{Ti}_2\text{O}_7$ [32, 33] are shown for comparison.

With the fitted CEF ground states and coupling strengths, we can determine the monopole parameters. The monopole charge $Q_m = 2\langle J_z \rangle g \mu_B / \sqrt{3}/2r_0$ can be calculated to be 3.28 and 3.42 $\mu_B/\text{\AA}$ for CdEr_2Se_4 and CdEr_2S_4 , respectively [3]. The chemical potential $v_0 = 2J_1 + (8/3)(1 + \sqrt{2/3})D$, which is half of the energy cost to create and unbind a monopole-antimonopole pair [9], is 2.93 K for CdEr_2Se_4 and 3.84 K for CdEr_2S_4 . Although the chemical potentials in CdEr_2X_4 are lower than that in $\text{Dy}_2\text{Ti}_2\text{O}_7$ (4.35 K), they are still more than two times higher than the energy cost $E_{\text{unbind}} = (8/3)\sqrt{2/3}D$ to unbind a monopole-antimonopole pair, locating both compounds in the same weakly correlated magnetolyte regime as $\text{Dy}_2\text{Ti}_2\text{O}_7$ [9].

Monopole dynamics in the low and high frequency regimes can be probed with ac-susceptibility [10, 32–34] and neutron spin echo spectroscopy [35, 36], respectively, and the representative results for CdEr_2Se_4 are shown in Fig. 3a and b. Fig. 3c summarizes the temperature dependence of the characteristic relaxation time $\tau = 1/2\pi f$ in CdEr_2X_4 , where the results for $\tau > 1 \times 10^{-3}$ s are extracted from the peak positions of the imaginary part of the ac-susceptibility $\chi''(T)$, the results for $10^{-5} > \tau > 10^{-7}$ s are obtained by fitting $\chi(\omega)$ to the Cole-Cole model [37], and the results for $\tau < 10^{-8}$ s are obtained

by fitting the neutron spin echo intermediate scattering function with $S(Q, t)/S(Q, 0) = A \exp[-t/\tau(T)]$ [35, 36]. The relaxation time in $\text{Dy}_2\text{Ti}_2\text{O}_7$ [32, 33] is also shown in Fig. 3c for comparison.

Firstly, we observe that at $T > 10$ K, the relaxation time in CdEr_2X_4 obeys the Orbach law of $\tau = \tau_0[\exp(\Delta/k_B T) - 1]$ [13], with the parameters $\tau_0 = 3.93(9) \times 10^{-11}$ s and $\Delta = 77.1$ K for CdEr_2Se_4 , and $\tau_0 = 2.73(5) \times 10^{-11}$ s and $\Delta = 96.3$ K for CdEr_2S_4 . The fitted excitation energies Δ in CdEr_2X_4 are much smaller than that of $\text{Dy}_2\text{Ti}_2\text{O}_7$ ($\Delta > 230$ K), which is due to their lower CEF excited states [13].

The Orbach behavior of the relaxation rate does not extend to the lowest temperature. Instead, at T in-between 2 and 5 K, a plateau region with $\tau \sim 4.9 \times 10^{-7}$ s, which was inaccessible in the previous susceptibility measurements [18], is observed for both CdEr_2Se_4 and CdEr_2S_4 , reminiscent of the $\tau \sim 2.6 \times 10^{-4}$ s quantum tunneling plateau in $\text{Dy}_2\text{Ti}_2\text{O}_7$ [10, 11, 33]. Such a similarity extends to even lower temperatures where the relaxation time starts rising again. As can be seen in Fig. 3c, at $T < 1$ K, the relaxation time in CdEr_2X_4 can be described by the Arrhenius law of $\tau_0 \exp(\Delta/k_B T)$, with parameters $\tau_0 = 1.01(1) \times 10^{-10}$ s and $\Delta = 10.07$ K for CdEr_2Se_4 , and $\tau_0 = 2.9(1) \times 10^{-10}$ s and $\Delta = 10.2(6)$ K for CdEr_2S_4 . Due to the limited data points for CdEr_2Se_4 , the fitted Δ value from Ref. [18] has been used. The activation energies in CdEr_2X_4 are very close to that of $\text{Dy}_2\text{Ti}_2\text{O}_7$, where the Arrhenius law with $\tau_0 = 3.07 \times 10^{-7}$ s and $\Delta = 9.93$ K has been observed in a similar temperature regime [32].

Despite the similar temperature evolution, the absolute values of the monopole relaxation rates in CdEr_2X_4 are about 10^3 times higher than that in $\text{Dy}_2\text{Ti}_2\text{O}_7$ for the whole measured quantum tunneling region, which cannot be simply accounted for by the difference of the monopole densities ρ . Assuming $\rho(T) \propto \exp(-v_0/k_B T)$, the monopole densities in CdEr_2X_4 are no more than 10 times higher than that of $\text{Dy}_2\text{Ti}_2\text{O}_7$ in the investigated quantum tunneling region. According to the $f \propto u\rho$ relation of the Debye-Hückel theory, there must be a two-orders increase of the monopole hopping rates u in CdEr_2X_4 .

Following Tomassello *et al.* [16], we analyze the perturbation effect of an internal transverse magnetic field on the CEF ground state doublet in CdEr_2Se_4 and CdEr_2S_4 . Due to the similar NN couplings [9], we expect similar internal field strengths in CdEr_2X_4 and $\text{Dy}_2\text{Ti}_2\text{O}_7$ [38]. The perturbed Hamiltonian can be written as:

$$\mathcal{H} = \sum_{lm} B_l^m \hat{O}_l^m + H \cos(\phi) \hat{J}_x + H \sin(\phi) \hat{J}_y, \quad (2)$$

where the y direction is along the C_2 axis and ϕ is the angle between the transverse field H and the x direction (see the inset of Fig. 4). Similar to the Dy^{3+} ions in $\text{Dy}_2\text{Ti}_2\text{O}_7$ [16], the Kramers degeneracy of the Er^{3+}

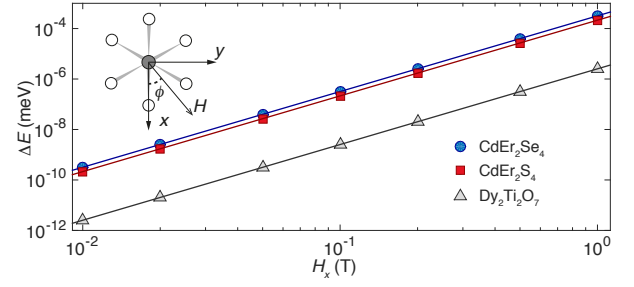


FIG. 4. (color online). Splittings of the CEF ground state doublet in CdEr_2Se_4 , CdEr_2S_4 , and $\text{Dy}_2\text{Ti}_2\text{O}_7$ under a perturbative magnetic field along the x direction. Definitions of the axes are shown in the inset.

ions causes a third-order dependence of the ground state splitting on the field strength in the perturbative regime: $\Delta E = \alpha [1 + A \cos(6\phi)] H^3$. Using the McPhase program [21], we directly diagonalize the Hamiltonian (2) and fit the coefficients to be $\alpha = 2.80 \times 10^{-4}$ (1.95×10^{-4}) [meV/T³] and $A = 0.136$ (0.098) for CdEr_2Se_4 (CdEr_2S_4). For $\text{Dy}_2\text{Ti}_2\text{O}_7$, using the CEF parameters of Ref. [39], the coefficients are calculated to be $\alpha = 2.14 \times 10^{-6}$ [meV/T³] and $A = 0.183$. As is compared in Fig. 4 for magnetic field along the x direction, the CEF ground state splittings in CdEr_2X_4 are indeed $\sim 10^2$ larger than that in $\text{Dy}_2\text{Ti}_2\text{O}_7$ under the same transverse magnetic field. Our results suggest that the increase of the monopole hopping rate is the main contribution to the very fast monopole dynamics in CdEr_2X_4 , and at the same time support the single-ion quantum tunneling process proposed in Ref. [16] as a general monopole hopping mechanism in dipolar spin ices.

This higher susceptibility of the Er^{3+} ions to transverse magnetic field is a property of the full CEF Hamiltonian, but might not be the only factor that contributes to the high monopole hopping rates in CdEr_2X_4 . As is listed in Tab. I, the CEF ground state doublets have relatively larger components of $|J_z\rangle$ with $|J_z| \leq 7/2$ compared to those of the pyrochlore titanates [39]. According to a microscopic analysis [40], such components might give rise to non-negligible multipolar interactions that can further increase the monopole hopping rates.

Dipolar spin ice states with fast monopole hopping rate enable the study of the magnetic Coulomb phase in a broader frequency regime. In particular, nonequilibrium phenomena such as the Wein effect [14, 41], which appear in $\text{Dy}_2\text{Ti}_2\text{O}_7$ at temperatures well below those measured here, may be modified. Also, thermal equilibration may be much faster in CdEr_2X_4 , facilitating the search for the intrinsic ground state and quantum effects in dipolar spin ices [42, 43].

In summary, neutron scattering investigations of the spin correlations in CdEr_2X_4 ($X = \text{Se}, \text{S}$) confirm they are the first spinels that realize dipolar spin ice states, such that their dynamics should be controlled by emer-

gent magnetic monopoles. The high temperature Orbach behavior observed in our neutron spin echo experiments gives way to fast monopole hopping dynamics at low temperature (compared to the pyrochlore titanate spin ice $\text{Dy}_2\text{Ti}_2\text{O}_7$). Comparison of monopole populations calculated using Coulomb gas parameters estimated from the diffuse scattering experiments and bulk properties, and monopole hopping rates calculated using the CEF Hamiltonian derived from our inelastic neutron scattering data, show that the main contribution to the fast monopole dynamics of CdEr_2X_4 is due to the much larger hopping rate. The successful reproduction of the very different relaxation rates in CdEr_2X_4 and $\text{Dy}_2\text{Ti}_2\text{O}_7$ using realistic Coulomb gas parameters and CEF Hamiltonians for each compound supports the general application of this method to the description of monopole hopping processes in dipolar spin ices.

We acknowledge valuable discussions with C. Castelnovo, M.J.P. Gingras, B. Tomasello, H. Kadowaki, G. Chen, M. Ruminy, J. Xu, J.S. White, A. Turrini, and J.-H. Chen. We also thank V. Markushin for help with the Merlin4 cluster. Our neutron scattering experiments were performed at the Institut Laue-Langevin ILL, Grenoble, France and the Swiss Spallation Neutron Source SINQ, Paul Scherrer Institut PSI, Villigen, Switzerland. The susceptibility measurements were carried out in the Laboratory for Scientific Developments and Novel Materials of PSI. The Monte Carlo simulations were performed on the Merlin4 cluster at PSI. This work was supported by the Swiss National Science Foundation under Grants No. 20021-140862, No. 20020-162626, and the SCOPES project No. IZ73Z0-152734/1. S. R. G. thanks EPSRC for financial support under EP/L019760/1.

* oksana.zaharko@psi.ch

† tom.fennell@psi.ch

- [1] C. L. Henley, *Ann. Rev. Condens. Matter Phys.* **1**, 179 (2010).
- [2] S. T. Bramwell and M. J. P. Gingras, *Science* **294**, 1495 (2001).
- [3] C. Castelnovo, R. Moessner, and S. L. Sondhi, *Nature (London)* **451**, 42 (2008).
- [4] T. Fennell, P. P. Deen, A. R. Wildes, K. Schmalzl, D. Prabhakaran, A. T. Boothroyd, R. J. Aldus, D. F. McMorrow, and S. T. Bramwell, *Science* **326**, 415 (2009).
- [5] D. J. P. Morris, D. A. Tennant, S. A. Grigera, B. Klemke, C. Castelnovo, R. Moessner, C. Czternasty, M. Meissner, K. C. Rule, J.-U. Hoffmann, K. Kiefer, S. Gerischer, D. Slobinsky, and R. S. Perry, *Science* **326**, 411 (2009).
- [6] S. R. Giblin, S. T. Bramwell, P. C. W. Holdsworth, D. Prabhakaran, and I. Terry, *Nat. Phys.* **7**, 252 (2011).
- [7] I. A. Ryzhkin, *J. Exp. Theo. Phys.* **101**, 481 (2005).
- [8] C. Castelnovo, R. Moessner, and S. L. Sondhi, *Phys. Rev. B* **84**, 144435 (2011).
- [9] H. D. Zhou, S. T. Bramwell, J. G. Cheng, C. R. Wiebe, G. Li, L. Balicas, J. A. Bloxsom, H. J. Silverstein, J. S. Zhou, J. B. Goodenough, and J. S. Gardner, *Nat. Commun.* **2**, 478 (2011).
- [10] J. Snyder, B. G. Ueland, J. S. Slusky, H. Karunadasa, R. J. Cava, and P. Schiffer, *Phys. Rev. B* **69**, 064414 (2004).
- [11] L. D. C. Jaubert and P. C. W. Holdsworth, *Nat. Phys.* **5**, 258 (2009).
- [12] L. D. C. Jaubert and P. C. W. Holdsworth, *J. Phys. Condens. Matter* **23**, 164222 (2011).
- [13] M. Ruminy, S. Chi, S. Calder, and T. Fennell, *Phys. Rev. B* **95**, 060414 (2017).
- [14] C. Paulsen, M. J. Jackson, E. Lhotel, B. Canals, D. Prabhakaran, K. Matsuhira, S. R. Giblin, and S. T. Bramwell, *Nat. Phys.* **10**, 135 (2014).
- [15] H. Takatsu, K. Goto, H. Otsuka, R. Higashinaka, K. Matsubayashi, Y. Uwatoko, and H. Kadowaki, *J. Phys. Soc. Jpn* **82**, 104710 (2013).
- [16] B. Tomasello, C. Castelnovo, R. Moessner, and J. Quintanilla, *Phys. Rev. B* **92**, 155120 (2015).
- [17] G. C. Lau, R. S. Freitas, B. G. Ueland, P. Schiffer, and R. J. Cava, *Phys. Rev. B* **72**, 054411 (2005).
- [18] J. Lago, I. Živković, B. Z. Malkin, J. Rodriguez Fernandez, P. Ghigna, P. Dalmas de Réotier, A. Yaouanc, and T. Rojo, *Phys. Rev. Lett.* **104**, 247203 (2010).
- [19] D. Reig-i Plessis, S. V. Geldern, A. A. Aczel, and G. J. MacDougall, *arXiv:1703.04267* (2017).
- [20] See Supplemental Materials for details on the sample preparation, impurities in CdEr_2Se_4 and spin correlations in CdEr_2S_4 .
- [21] M. Rotter, *J. Mag. Magn. Mater.* **272-276**, E481 (2004).
- [22] Y.-P. Huang, G. Chen, and M. Hermele, *Phys. Rev. Lett.* **112**, 167203 (2014).
- [23] Y.-D. Li, X. Wang, and G. Chen, *Phys. Rev. B* **94**, 201114 (2016).
- [24] G. Ehlers, J. R. Stewart, A. R. Wildes, P. P. Deen, and K. H. Andersen, *Rev. Sci. Instr.* **84**, 093901 (2013).
- [25] H. Kadowaki, Y. Ishii, K. Matsuhira, and Y. Hinatsu, *Phys. Rev. B* **65**, 144421 (2002).
- [26] I. Mirebeau and I. Goncharenko, *Journal of Physics: Condensed Matter* **16**, S653 (2004).
- [27] A. M. Hallas, J. A. M. Paddison, H. J. Silverstein, A. L. Goodwin, J. R. Stewart, A. R. Wildes, J. G. Cheng, J. S. Zhou, J. B. Goodenough, E. S. Choi, G. Ehlers, J. S. Gardner, C. R. Wiebe, and H. D. Zhou, *Phys. Rev. B* **86**, 134431 (2012).
- [28] T. Yavorskii, T. Fennell, M. J. P. Gingras, and S. T. Bramwell, *Phys. Rev. Lett.* **101**, 037204 (2008).
- [29] B. Bauer, L. D. Carr, H. G. Evertz, A. Feiguin, J. Freire, S. Fuchs, L. Gamper, J. Gukelberger, E. Gull, S. Guertler, A. Hehn, R. Igarashi, S. V. Isakov, D. Koop, P. N. Ma, P. Mates, H. Matsuo, O. Parcollet, G. Pawłowski, J. D. Picon, L. Pollet, E. Santos, V. W. Scarola, U. Schollwöck, C. Silva, B. Surer, S. Todo, S. Trebst, M. Troyer, M. L. Wall, P. Werner, and S. Wessel, *J. Stat. Mech.: Theo. and Exp.* **2011**, P05001 (2011).
- [30] B. C. den Hertog and M. J. P. Gingras, *Phys. Rev. Lett.* **84**, 3430 (2000).
- [31] H. D. Zhou, J. G. Cheng, A. M. Hallas, C. R. Wiebe, G. Li, L. Balicas, J. S. Zhou, J. B. Goodenough, J. S. Gardner, and E. S. Choi, *Phys. Rev. Lett.* **108**, 207206 (2012).
- [32] L. R. Yaraskavitch, H. M. Revell, S. Meng, K. A. Ross, H. M. L. Noad, H. A. Dabkowska, B. D. Gaulin, and J. B.

- Kycia, Phys. Rev. B **85**, 020410 (2012).
- [33] K Matsuhira and Y Hinatsu and T Sakakibara, J. Phys. Condens. Matter **13**, L737 (2001).
 - [34] J. A. Quilliam, L. R. Yaraskavitch, H. A. Dabkowska, B. D. Gaulin, and J. B. Kycia, Phys. Rev. B **83**, 094424 (2011).
 - [35] G. Ehlers, A. L. Cornelius, M. Orendác, M. Kajnaková, T. Fennell, S. T. Bramwell, and J. S. Gardner, J. Phys. Condens. Matter **15**, L9 (2003).
 - [36] G. Ehlers, A. L. Cornelius, T. Fennell, M. Koza, S. T. Bramwell, and J. S. Gardner, J. Phys. Condens. Matter **16**, S635 (2004).
 - [37] L. Bovo, J. A. Bloxsom, D. Prabhakaran, G. Aeppli, and S. T. Bramwell, Nat. Commun. **4**, 1535 (2013).
 - [38] G. Sala, C. Castelnovo, R. Moessner, S. L. Sondhi, K. Kitagawa, M. Takigawa, R. Higashinaka, and Y. Maeno, Phys. Rev. Lett. **108**, 217203 (2012).
 - [39] M. Ruminy, E. Pomjakushina, K. Iida, K. Kamazawa, D. T. Adroja, U. Stuhr, and T. Fennell, Phys. Rev. B **94**, 024430 (2016).
 - [40] J. G. Rau and M. J. P. Gingras, Phys. Rev. B **92**, 144417 (2015).
 - [41] C. Paulsen, S. R. Giblin, E. Lhotel, D. Prabhakaran, G. Balakrishnan, K. Matsuhira, and S. T. Bramwell, Nat Phys **12**, 661 (2016).
 - [42] D. Pomaranski, L. R. Yaraskavitch, S. Meng, K. A. Ross, H. M. L. Noad, H. A. Dabkowska, B. D. Gaulin, and J. B. Kycia, Nat. Phys. **9**, 353 (2013).
 - [43] P. Henelius, T. Lin, M. Enjalran, Z. Hao, J. G. Rau, J. Altosaar, F. Flicker, T. Yavors'kii, and M. J. P. Gingras, Phys. Rev. B **93**, 024402 (2016).

Dipolar spin ice states with fast monopole hopping rate in CdEr_2X_4 ($\text{X} = \text{Se}, \text{S}$) Supplementary Information

Sample preparation

The polycrystalline samples of CdEr_2X_4 ($\text{X} = \text{Se}, \text{S}$) were prepared by solid state synthesis from binary Er and Cd selenides and sulfides. The binary CdX were synthesized from the elemental Cd-114, while the Er_2X_3 were prepared from the high purity Er chips (99.9 %, Chempur) and elemental S (99.999 %, Strem Chemicals) or Se (99.999 %, Alfa Aesar). Selenium was additionally purified by zone melting. To reduce the oxide impurity Er_2O_3 which easily forms in the open air, all preparation procedures (quartz ampoule filling, reacted mixture regrinding, and pellets pressing) were performed in an argon box with an O_2 and H_2O content of ~ 1 ppm. To reach full homogeneity, at least three sintering cycles of synthesis of the binary Er and Cd chalcogenides were performed. The phase purity of the binary compounds was checked by x-ray powder diffraction. Finally, the ternary $^{114}\text{CdEr}_2\text{X}_4$ were prepared by two consecutive synthesis at 800°C for one week each.

The single crystals of CdEr_2X_4 were grown by the chemical transport reactions method. As starting materials the preliminary synthesized polycrystalline powders were used. For the growth, several transport agents were probed, including chlorine, bromine and iodine. We found that only the iodine is suitable for the growth of the ternary phase, while in the case of chlorine or bromine the final product contained mainly binary Cd and Er chalcogenides. The growth process was performed in a two-zone furnace with the hot part temperature of 950°C and a temperature gradient of about 40°C . The time for one crystal growth experiment was between 1 and 1.5 months. As a result, the octahedron-like single crystals with dimension up to 1.5 mm of the edge were obtained.

Sample characterizations and impurities in CdEr_2Se_4

The purity content and crystal structure of the samples were checked by conventional X-ray powder diffraction on polycrystalline samples and crashed single crystals. Fig. S1 shows the refinement results for the $^{114}\text{CdEr}_2\text{Se}_4$ and $^{114}\text{CdEr}_2\text{S}_4$ polycrystalline samples using cubic $Fd\bar{3}m$ symmetry expected for the normal spinel structure. Table S1 lists the refined size of the unit cell, fractional position for the Se or S ions, and the goodness-of-fit parameters. No inversion between Cd and Er can be observed. No peaks from impurities are detectable, implying their tiny amount. However, at low temperatures, weak magnetic Bragg peaks of the Er_xSe_y impurities [S1] are discernible in the neutron diffuse scattering experiment shown in Fig. 2 of the main text.

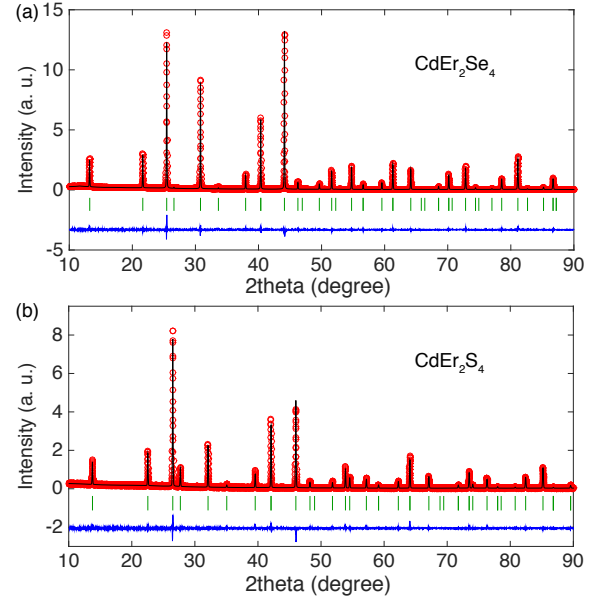


FIG. S1. Refinement results of the X-ray diffraction data measured at room temperature for (a) $^{114}\text{CdEr}_2\text{Se}_4$ polycrystalline sample and (b) $^{114}\text{CdEr}_2\text{S}_4$ polycrystalline sample. Data points are shown as red circles. The calculated pattern is shown as the black solid line. The vertical bars show the positions of the Bragg peaks. And the blue line at the bottom shows the difference of data and calculated intensities.

The extrinsic origin of the weak Bragg peaks is evident in their different temperature dependence compared with the broad diffuse scattering. Fig. S2 shows the non-polarized neutron diffraction results measured on D20 at ILL with the 20 K measurement subtracted as the background. The setup with 2.41 \AA incoming neutron wavelength was employed. As can be seen in the inset of Fig. S2a and Fig. S2b, intensities of the sharp peaks saturate at temperatures below 0.8 K while the broad peaks from the diffuse scattering continue their growth, evidencing their different origins.

Dipolar spin ice state in CdEr_2S_4

Ice-correlations similar to that of CdEr_2Se_4 are also observed in CdEr_2S_4 . Fig. S3 presents the non-polarized neutron diffuse scattering results for CdEr_2S_4 measured on DMC at PSI with the setup of 2.46 \AA incoming neutron wavelength. The 50 K measurement has been subtracted as the background. Similar to the CdEr_2Se_4 results shown in Fig. 2 of the main text, broad peaks at ~ 0.6 , 1.4 , and 2.5 \AA^{-1} are observed at low temperatures, which suggest similar ice-correlations in CdEr_2S_4 .

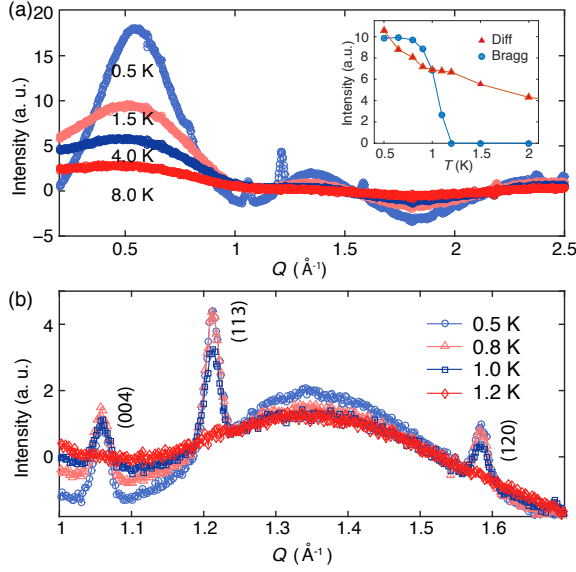


FIG. S2. (a) Non-polarized neutron diffraction results for CdEr_2Se_4 measured on D20 at 0.5, 1.5, 4, and 8 K. The inset compares the temperature dependence of the Bragg peak intensity at 1.22 \AA^{-1} and the integrated diffuse scattering intensity in $1.325 < Q < 1.375 \text{ \AA}^{-1}$. (b) Detailed temperature dependence of the intensities in the region of $1 \sim 1.7 \text{ \AA}^{-1}$ in between 0.5 and 1.2 K. The Bragg peaks are indexed for the impurity of Er_2Se_3 .

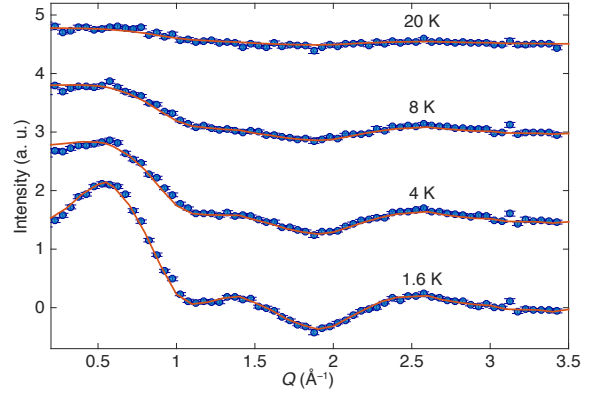


FIG. S3. Non-polarized neutron diffuse scattering results for CdEr_2S_4 measured at 1.6, 4, 8, and 20 K with the 50 K data subtracted as the background. The data at 4, 8, and 20 K are shifted by 1.5, 3.0, and 4.5 along the y axis, respectively. The mean-field calculation results assuming only dipolar interactions are shown as the solid lines.

Mean-field calculations were performed to confirm the ice-correlations in CdEr_2S_4 [S2]. Denoting the α component ($\alpha = x, y, z$) of the ν -th unit-length spin ($\nu = 1, 2, 3, 4$) in the n -th primitive unit cell as $S_{n,\nu,\alpha}$, the Hamiltonian on the pyrochlore lattice can be explicitly expressed as:

$$\begin{aligned} \mathcal{H} = & -E_a \sum_{n,\nu} \left[(\hat{n}_\nu \cdot S_{n,\nu})^2 - |S_{n,\nu}|^2 \right] - J_1 \sum_{\langle n,\nu;n',\nu' \rangle} S_{n,\nu} \cdot S_{n',\nu'} \\ & + Dr_0^3 \sum_{\langle n,\nu;n',\nu' \rangle} \left[\frac{S_{n,\nu} \cdot S_{n',\nu'}}{|r_{n,\nu;n',\nu'}|^3} - \frac{3(S_{n,\nu} \cdot r_{n,\nu;n',\nu'})(S_{n',\nu'} \cdot r_{n,\nu;n',\nu'})}{|r_{n,\nu;n',\nu'}|^5} \right] \\ = & - \sum_{n,\nu,\alpha;n',\nu',\beta} J_{n,\nu,\alpha;n',\nu',\beta} S_{n,\nu,\alpha} S_{n',\nu',\beta}, \end{aligned} \quad (1)$$

where the E_a term represents the easy-axis anisotropy and \hat{n}_ν is the unit vector along the easy axis of the ν -th spin. Fourier transform of the real-space coupling $J_{n,\nu,\alpha;n',\nu',\beta}$ leads to the 12×12 coupling matrix $J_{k;\nu,\alpha;\nu',\beta}$ in reciprocal space, which is then diagonalized:

$$\sum_{\nu',\beta} J_{k;\nu,\alpha;\nu',\beta} u_{k;\nu',\beta}^{(\rho)} = \lambda_k^{(\rho)} u_{k;\nu,\alpha}^{(\rho)}, \quad (2)$$

where $\lambda_k^{(\rho)}$ with $\rho = 1, 2, \dots, 12$ denotes the eigenvalues and $u_k^{(\rho)}$ denotes the corresponding eigenvectors. The global maximum of $\lambda_k^{(\rho)}$ determines the long-range order transition under the mean-field approximation, with the

transition temperature T_c as:

$$k_B T_c = \frac{2}{3} [\lambda_k^{(\rho)}]_{\max}. \quad (3)$$

The paramagnetic susceptibility at $T_{\text{MF}} > T_c$ can be

TABLE S1. Refinement results of the X-ray diffraction data for CdEr_2Se_4 and CdEr_2S_4 . The listed parameters are the refined size of the unit cell a , fractional position x of the $X = \text{Se}$ or S ions, and the goodness-of-fit R_p , R_{wp} , and χ^2 .

	a (Å)	X (x)	R_p	R_{wp}	χ^2
CdEr_2Se_4	11.6097(1)	0.2566(1)	13.0	14.6	2.16
CdEr_2S_4	11.1527(1)	0.2589(2)	19.7	19.1	1.89

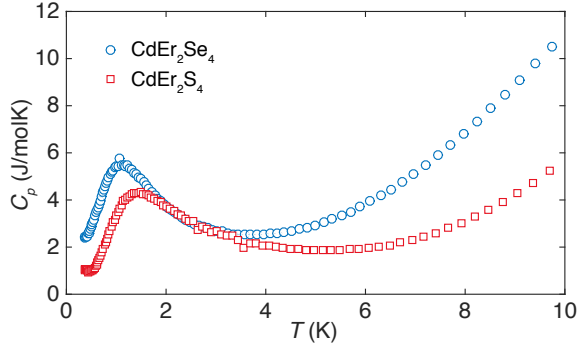


FIG. S4. Specific heat for CdEr_2Se_4 and CdEr_2S_4 single crystals. Tails at the lowest temperature might be due to impurities.

approximated by the eigenvalues and eigenfunctions:

$$\chi_{k;\nu,\alpha;\nu',\beta} = \frac{N\mu^2}{V} \sum_{\rho} \frac{u_{k;\nu,\alpha}^{(\rho)} u_{k;\nu',\beta}^{(\rho)*}}{3k_{\text{B}}T_{\text{MF}} - 2\lambda_k^{(\rho)}}, \quad (4)$$

where N is the total number of the unit cell, V is the volume of the system, and μ is the size of the magnetic moment. The cross section of the magnetic scattering can be expressed as:

$$\begin{aligned} \frac{d\sigma}{d\Omega}(Q = \tau + k) &= Pf(Q)^2 k_{\text{B}}T \sum_{\alpha,\beta,\nu,\nu'} \left(\delta_{\alpha\beta} - \hat{Q}_{\alpha} \hat{Q}_{\beta} \right) \\ &\times \chi_{k;\nu,\alpha;\nu',\beta} \cos[\tau \cdot (r_{\nu} - r_{\nu'})] - Kf(Q)^2, \end{aligned} \quad (5)$$

where P is a constant, $f(Q)$ is the magnetic form factor, τ is the reciprocal lattice vector, and r_{ν} denotes the position of the ν -th atom in the first primitive cell. The additional term of $Kf(Q)^2$ accounts for the subtracted spin correlations at 50 K.

To account for the Ising character of the Er^{3+} spin, a high anisotropy of $E_a = 810$ K was used. The dipolar interactions with $D = 0.690$ K was truncated beyond the length of 5 unit cells. Since T_c is an effective temperature that can be different from the real ordering temperature, the mean-field temperature T_{MF} was used as a fitting parameter [S2]. Fig. S3 presents the fitted results with $J_1 = 0$. In this case, T_c is calculated to be 1.8 K, and the fitted $T_{\text{MF}} = 2.0, 2.9, 4.8$, and 16.8 K for the data measured at 1.6, 4, 8, and 20 K, respectively. Thus the ice-correlation is proved to exist in CdEr_2S_4 .

In our mean-field calculation, the variance of J_1 does not affect the goodness-of-fit as long as $J_1/3 + 5D/3 > 0$. To obtain the monopole chemical potential, we measured the specific heat C_p for CdEr_2S_4 single crystals. As is shown in Fig. S4, the $C_p(T)$ maximum of CdEr_2S_4 is at ~ 1.4 K, which enable us to fix the monopole chemical potential to 3.84 K in CdEr_2S_4 (see main text).

* oksana.zaharko@psi.ch

† tom.fennell@psi.ch

[S1] S. Calder and T. Fennell and W. Kockelmann and G. C. Lau and R. J. Cava and S. T. Bramwell, J. Phys. Condens. Matt. **22**, 116007 (2010).

[S2] H. Kadowaki, Y. Ishii, K. Matsuhira, and Y. Hinatsu, Phys. Rev. B **65**, 144421 (2002).